Composite Structures 109 (2014) 68–74

Contents lists available at ScienceDirect

Composite Structures

journal homepage: www.elsevier.com/locate/compstruct

Mechanical properties of a hollow-cylindrical-joint honeycomb

Qiang Chen [a], Nicola Pugno [b,c,d], Kai Zhao [e], Zhiyong Li [a,*]

[a] Biomechanics Laboratory, School of Biological Science and Medical Engineering, Southeast University, 210096 Nanjing, PR China
[b] Laboratory of Bio-Inspired & Graphene Nanomechanics, Department of Civil, Environmental and Mechanical Engineering, University of Trento, I-38123 Trento, Italy
[c] Center for Materials and Microsystems, Fondazione Bruno Kessler, I-38123 Trento, Italy
[d] School of Engineering and Materials Science, Queen Mary Univerisity of London, Mile End Road, London, E1 4NS, UK
[e] Institute of Geotechnical Engineering, Nanjing University of Technology, 210009 Nanjing, PR China

ARTICLE INFO

Article history:
Available online 25 October 2013

Keywords:
Hollow-cylindrical-joint honeycomb
Young's modulus
Poisson's ratio
Stress intensity factor
Strength

ABSTRACT

In this paper, we constructed a new honeycomb by replacing the three-edge joint of the conventional regular hexagonal honeycomb with a hollow-cylindrical joint, and developed a corresponding theory to study its mechanical properties, *i.e.*, Young's modulus, Poisson's ratio, fracture strength and stress intensity factor. Interestingly, with respect to the conventional regular hexagonal honeycomb, its Young's modulus and fracture strength are improved by 76% and 303%, respectively; whereas, for its stress intensity factor, two possibilities exist for the maximal improvements which are dependent of its relative density, and the two improvements are 366% for low-density case and 195% for high-density case, respectively. Moreover, a minimal Poisson's ratio exists. The present structure and theory could be used to design new honeycomb materials.

1. Introduction

Honeycomb or foam structures extensively exist in natural materials, *e.g.* honeycomb [1], cancellous bone in animal skeletons and tree or grass stems [2]. From the mechanical point of view, their mechanical properties (such as light-weight, high-strength and super-tough) are linked to their optimal structures by Nature, which hints people to design different multifunctional materials [3–6]. To this end, a considerable number of scientists and engineers invented varieties of porous materials and investigated their mechanical properties. For example, mechanical properties of hierarchical nanohoneycomb or nanofoam materials, for which surface effect was included, were studied [7,8]. It is found that the elastic modulus and strength decrease as hierarchical level number increases. Also the sandwich walls with core struts in lattice structures have superior mechanical properties to that with solid walls [9]. Similarly, substituted solid cell walls of the conventional hexagonal honeycomb with equal-mass honeycomb lattice, the Young's modulus of new structures is optimized and improved by 75% comparing to the conventional hexagonal honeycomb [10]; also, by replacing the three-edge joint of the regular hexagonal honeycomb with a hollow hexagonal prism, the Young's modulus of the fractal-like structure is optimized [11]. Besides, replaced the solid cell walls of the conventional hexagonal honeycomb with a equal-mass re-entrant negative Poisson's ratio honeycomb [12], the Young's modulus of the new structure is again dramatically improved.

Regarding the fracture behavior of honeycomb-like structures, not like the theory for continuum media, the common method is employing the stress field ahead of crack tip, then, performing structural analysis. There exist such models in literatures [13–15]. Maiti et al. [13] and Choi and Lakes [14] used the conventional singular stress field and the nonsingular stress field for blunt cracks to calculate the axial force acting on the first vertical cell ahead of crack tip, respectively, and both the two models derived fracture strength first and then stress intensity factor. However, Choi and Sankar [15] calculated the axial force and bending moment acting on the first vertical cell ahead of crack tip, and selected an effective portion of crack tip stress field considering the existence of singularity, then, the stress intensity factor was directly obtained.

In this paper, by observing natural honeycombs, we found that the cell walls of the natural honeycombs have varying cross-sections, and the thickness reaches a maximum at both ends of cell walls (marked by circle in Fig. 1a). It is speculated that the moments at these ends bear the greatest bending moment, and honeybees strengthen their nests by introducing more materials to the weakest points, exactly like the specifications of building design, in which more steel bars and concrete are placed at load-bearing positions in beams. Meanwhile, considering the superior mechanical efficiency of natural porous structures to solid materials [8,10,11], we proposed a so-called hollow-cylindrical-joint honeycomb (Fig. 1c) by replacing the three-edge joint with a hollow

* Corresponding author. Tel./fax: +86 2583792620.
E-mail address: zylicam@gmail.com (Z. Li).

0263-8223/$ - see front matter © 2013 Elsevier Ltd. All rights reserved.
http://dx.doi.org/10.1016/j.compstruct.2013.10.025

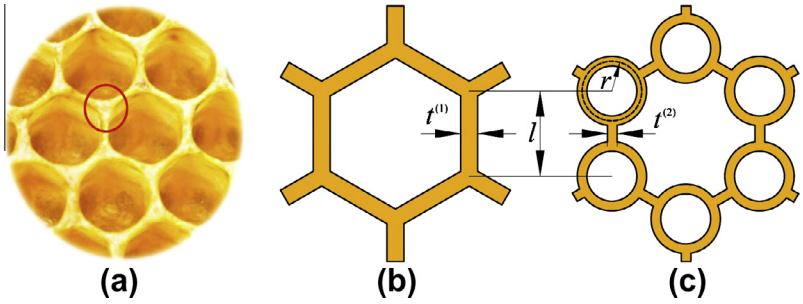

Fig. 1. (a) Natural honeycomb; (b) conventional regular hexagonal honeycomb; (c) hollow-cylindrical-joint honeycomb.

cylinder instead of the hollow hexagonal prism reported in Ref. [11]. The related structure can be regarded as the derivative structure from the family of center-symmetrical honeycombs in Ref. [16]. In particular, the out-of-plane properties of the tetrachiral and hexachiral honeycomb family were well studied by experiments and finite element method, and the results showed that buckling strength of the honeycombs could be optimized for applications in some fields [16]. For the present structure, its Young's modulus and Poisson's ratio was derived basing on Castigliano's theorem, and its stress intensity factor and strength were calculated by invoking the quantized fracture mechanics (QFM) thanks to the discrete feature of the honeycomb. In the following sections, the mechanical properties of the honeycomb with respect to those of the conventional regular hexagonal honeycomb are studied and discussed in detail.

2. Structural theory

Regarding the relative density of the conventional regular hexagonal honeycomb (Fig. 1b), it is approximately expressed as $\bar{\rho}^{(1)} = \frac{\rho^{(1)}}{\rho^s} = \frac{2}{\sqrt{3}}\left(\frac{t^{(1)}}{l}\right)$, where, ρ^s is the density of constituent materials, $t^{(1)}$ is the thickness of cell walls, the superscript (1) denotes the conventional regular hexagonal honeycomb, and its mechanical properties dependent of $t^{(1)}/l$ are systematically derived by Gibson and Ashby [17]. Different from the above expression of relative density, here, it is precisely expressed by including a quadratic term, *i.e.*,

$$\bar{\rho}^{(1)} = \frac{1}{3}\left[-\left(\frac{t^{(1)}}{l}\right) + 2\sqrt{3}\right]\left(\frac{t^{(1)}}{l}\right).$$

As for the relative density of the hollow-cylindrical-joint structure denoted by the superscript (2), we calculate it by a geometrical analysis as,

$$\bar{\rho}^{(2)} = \frac{\rho^{(2)}}{\rho^s} = \frac{2}{3\sqrt{3}}\left[-3\left(\frac{t^{(2)}}{l}\right) + 2(2\pi - 3)\left(\frac{r}{l}\right) + 3\right]\left(\frac{t^{(2)}}{l}\right) \tag{1}$$

where $t^{(2)}$ is the thickness of structure's cell walls, r is the radius of the circular joint (Fig. 1c). It is noted that the structure's geometry requires $0 < t^{(2)}/r \leqslant 2$ and $0 < r/l < 0.5$.

2.1. Young's modulus

A representative unit (Fig. 2) is selected and considered as the sum of three components, *i.e.*, semicircle *AD*, beams *BC* and *DE*. Under the uniaxially external tensile stress, no rotation and horizontal displacement occurs at the end *A*, thus, the boundary condition of the end *A* is simplified to be guided, see Fig. 2. The force P_0 acting on the end *C* of the beam *BC* is equivalent to $P_0 = \sqrt{3}\sigma^{(2)}bl/2$, where $\sigma^{(2)}$ is the external stress, b is the out-of-plane depth of the honeycomb, and l is the length of cell walls.

For the representative unit *ABCDE*, according to its geometrical components, the total strain energy stored in it is correspondingly composed by three components,

$$U = U_{AD} + U_{BC} + U_{DE} \tag{2}$$

where U_{AD}, U_{BC} and U_{DE} are elastic strain energies stored in the semicircle *AD*, beams *BC* and *DE*, respectively. Furthermore, the semicircle *AD* is divided into two subsections: one is *AB* and the other *BD*. Performing force analysis (Fig. 2), we obtain inner forces in the subsection *AB*: $N_{\mathrm{I}} = R\cos\theta$, $V_{\mathrm{I}} = R\sin\theta$, $M_{\mathrm{I}} = -M_A + Rr(1-\cos\theta)$ when $0 < \theta \leqslant \pi/3$ and in section *BD*: $N_{\mathrm{II}} = -R\cos\theta + P_0\sin\theta$, $V_{\mathrm{II}} = -R\sin\theta - P_0\cos\theta$, $M_{\mathrm{II}} = M_A + M_0 + P_0 r\left(\frac{\sqrt{3}}{2} - \sin\theta\right) - Rr(1-\cos\theta)$, when $\pi/3 \leqslant \theta \leqslant \pi$. Thus, the elastic strain energy in the semicircle *AD* is calculated as:

$$\begin{aligned}
U_{AD} &= \frac{r}{2E^sA^{(2)}}\left\{\left[\int_0^{\frac{\pi}{3}} N_{\mathrm{I}}^2 d\theta + \int_{\frac{\pi}{3}}^{\pi} N_{\mathrm{II}}^2 d\theta\right] + k\frac{E}{G}\left[\int_0^{\frac{\pi}{3}} V_{\mathrm{I}}^2 d\theta + \int_{\frac{\pi}{3}}^{\pi} V_{\mathrm{II}}^2 d\theta\right]\right. \\
&\quad \left. + \frac{A}{I}\left[\int_0^{\frac{\pi}{3}} M_{\mathrm{I}}^2 d\theta + \int_{\frac{\pi}{3}}^{\pi} M_{\mathrm{II}}^2 d\theta\right]\right\} \\
&= \frac{r}{2E^sA^{(2)}}\left(\frac{t^{(2)}}{l}\right)^{-2} \\
&\quad \times \left\{\begin{array}{l}
12\left[\pi\left(\frac{M_A}{l}\right)^2 + \left(\frac{4\pi}{3}\left(\frac{M}{l}\right) - 3P_0\left(\frac{r}{l}\right)\right)\left(\frac{M_A}{l}\right) - 2\pi\left(\frac{r}{l}\right)\left(\frac{M_A}{l}\right)R\right] \\
+R\left[45P_0\left(\frac{r}{l}\right)^2 - 4(4\pi + 3\sqrt{3})\left(\frac{M}{l}\right)\left(\frac{r}{l}\right) + \frac{3}{4}(1 - 2k(1+v_s))P_0\left(\frac{t^{(2)}}{l}\right)^2\right] \\
+\frac{\pi}{2}R^2\left[36\left(\frac{r}{l}\right)^2 + (1 + 2k(1+v_s))\left(\frac{t^{(2)}}{l}\right)^2\right] \\
+\left[8\pi\left(\frac{M}{l}\right)^2 - 36P_0\left(\frac{M}{l}\right)\left(\frac{r}{l}\right) + P_0^2\left(4\pi + \frac{3\sqrt{3}}{2}\right)\left(\frac{r}{l}\right)^2\right. \\
\quad \left. + P_0^2\left(\left(\frac{\pi}{3} + \frac{\sqrt{3}}{8} + 2k(1+v_s)\left(\frac{\pi}{3} - \frac{\sqrt{3}}{8}\right)\right)\left(\frac{t^{(2)}}{l}\right)^2\right]
\end{array}\right\}
\end{aligned} \tag{3}$$

where $M = M_0 + \frac{\sqrt{3}}{2}P_0 r$ is a defined moment.

According to Castigliano's first theorem and boundary conditions of the end *A*, the conditions $\partial U_{AD}/\partial R = 0$ and $\partial U_{AD}/\partial M_A = 0$ hold, then, an equation system with respect to two dimensionless reaction forces $\lambda_1 = Rl/M$ and $\lambda_2 = M_A/M$ emerges:

$$\begin{cases} \lambda_2 + C_1\lambda_1 + C_2 = 0 \\ \lambda_2 + C_3\lambda_1 + C_4 = 0 \end{cases} \tag{4}$$

where,

$$\begin{cases}
C_1 = -\frac{1}{24}\left(\frac{r}{l}\right)^{-1}\left[36\left(\frac{r}{l}\right)^2 + (1 + 2k(1+v_s))\left(\frac{t^{(2)}}{l}\right)^2\right] \\
C_2 = -\frac{1}{24\pi}\left(\frac{r}{l}\right)^{-1}\left[45\left(\frac{P_0 l}{M}\right)\left(\frac{r}{l}\right)^2 - 4(4\pi + 3\sqrt{3})\left(\frac{r}{l}\right) + \frac{3}{4}(1 - 2k(1+v_s))\left(\frac{P_0 l}{M}\right)\left(\frac{t^{(2)}}{l}\right)^2\right] \\
C_3 = -\frac{r}{l} \\
C_4 = \left[\frac{2}{3} - \frac{3}{2\pi}\left(\frac{P_0 l}{M}\right)\left(\frac{r}{l}\right)\right]
\end{cases}$$

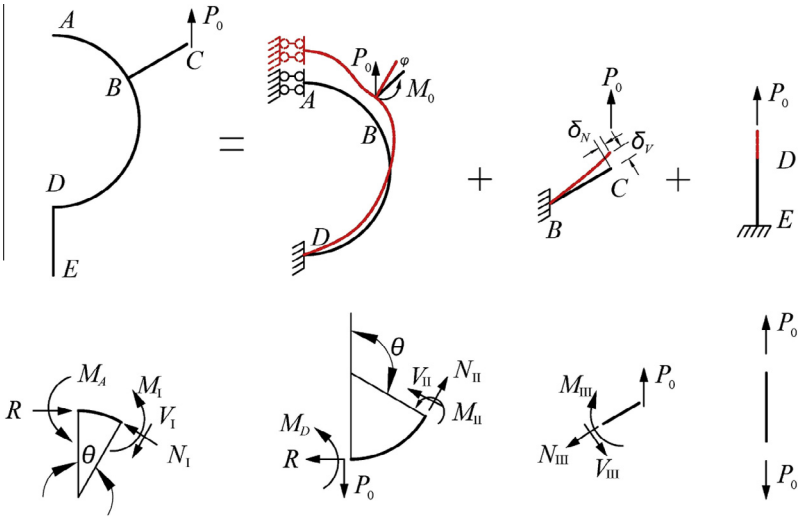

Fig. 2. Force analysis in a representative unit. Note that the red curves denote the after-deformed structures. (For interpretation of colour in this figure legend, the reader is referred to the web version of this article.)

solving the system, we obtain $\lambda_1 = -(C_2 - C_4)/(C_1 - C_3)$ and $\lambda_2 = (C_2C_3 - C_1C_4)/(C_1 - C_3)$. Then, the strain energy by Eq. (3) can be calculated with the known forces P_0 and M_0. For the present structure in Fig. 2, the two forces P_0 and M_0 satisfy $M_0 = \frac{\sqrt{3}}{2}P_0\left(\frac{l}{2} - r\right)$, *i.e.*, $\frac{P_0 l}{M} = \frac{4}{\sqrt{3}}$. Then, the strain energy in *ABCDE* is expressed as:

$$U_{AD} = \frac{P_0^2 r}{2E^s A^{(2)}}\left(\frac{t^{(2)}}{l}\right)^{-2} \times \left\{\begin{array}{l} 3\left[\frac{3\pi}{4}\lambda_2^2 - \frac{3\pi}{2}\left(\frac{r}{l}\right)\lambda_1\lambda_2 + \left(\pi - 3\sqrt{3}\left(\frac{r}{l}\right)\right)\lambda_2\right] \\ +\frac{\sqrt{3}}{4}\lambda_1\left[45\left(\frac{r}{l}\right)^2 - (9+4\sqrt{3}\pi)\left(\frac{r}{l}\right) + \frac{3}{4}(1-2k(1+\nu_s))\left(\frac{t^{(2)}}{l}\right)^2\right] \\ +\frac{3\pi}{32}\lambda_1^2\left[36\left(\frac{r}{l}\right)^2 + (1+2k(1+\nu_s))\left(\frac{t^{(2)}}{l}\right)^2\right] \\ +\left[\frac{3\pi}{2} - 9\sqrt{3}\left(\frac{r}{l}\right) + \left(4\pi + \frac{3\sqrt{3}}{2}\right)\left(\frac{r}{l}\right)^2 + \left(\left(\frac{\pi}{3} + \frac{\sqrt{3}}{8}\right)\right.\right. \\ \left.\left. +2k(1+\nu_s)\left(\frac{\pi}{3} - \frac{\sqrt{3}}{8}\right)\right)\left(\frac{t^{(2)}}{l}\right)^2\right] \end{array}\right\} \quad (5)$$

For the oblique cantilever beam *BC*, the inner forces are expressed as $N_{III} = P_0/2$, $V_{III} = \sqrt{3}P_0/2, M_{III} = \frac{\sqrt{3}P_0}{2}\left[\left(\frac{l}{2} - r\right) - x\right]$. It is noted that the moments at the joint *B* are balanced, *i.e.*, $M_{III}(0) = M_I\left(\frac{\pi}{3}\right) + M_{II}\left(\frac{\pi}{3}\right)$, which proves the correct force analysis to some extent. Correspondingly, its elastic strain energy is expressed as:

$$\begin{aligned} U_{BC} &= \frac{1}{2E^s A^{(2)}}\left[\int_0^{\left(\frac{l}{2}-r\right)} N_{III}^2 dx + k\frac{E}{G}\int_0^{\left(\frac{l}{2}-r\right)} V_{III}^2 dx + \frac{A}{I}\int_0^{\left(\frac{l}{2}-r\right)} M_{III}^2 dx\right] \\ &= \frac{P_0^2 r}{2E^s A^{(2)}}\left(\frac{t^{(2)}}{l}\right)^{-2}\left(\frac{l}{2r} - 1\right) \\ &\quad \times \left[3\left(\frac{1}{2} - \frac{r}{l}\right)^2 + \frac{1}{4}(1+6k(1+\nu_s))\left(\frac{t^{(2)}}{l}\right)^2\right] \end{aligned} \quad (6)$$

For the vertical cantilever beam *DE*, only axial deformation occurs, and thus, its elastic strain energy is easily expressed as:

$$U_{DE} = \frac{P_0^2 l}{2E^s A^{(2)}} \quad (7)$$

Substituting Eqs. (5)–(7) into Eq. (2), the total elastic strain energy *U* is derived. Again, employing Castigliano's first theorem, the displacement of the beam end *C* in the force direction is derived as,

$$\Delta_V = \frac{\partial U}{\partial P_0} = \frac{P_0 l}{E^s A^{(2)}}\left(\frac{l}{t^{(2)}}\right)^2 f\left(\frac{r}{l}, \frac{t^{(2)}}{l}\right) \quad (8)$$

where,

$$\begin{aligned} f\left(\frac{r}{l}, \frac{t^{(2)}}{l}\right) &= \left(\frac{r}{l}\right) \times \left\{\begin{array}{l} 3\left[\frac{3\pi}{4}\lambda_2^2 - \frac{3\pi}{2}\left(\frac{r}{l}\right)\lambda_1\lambda_2 + \left(\pi - 3\sqrt{3}\left(\frac{r}{l}\right)\right)\lambda_2\right] \\ +\frac{\sqrt{3}}{4}\lambda_1\left[45\left(\frac{r}{l}\right)^2 - (9+4\sqrt{3}\pi)\left(\frac{r}{l}\right) + \frac{3}{4}(1-2k(1+\nu_s))\left(\frac{t^{(2)}}{l}\right)^2\right] \\ +\frac{3\pi}{32}\lambda_1^2\left[36\left(\frac{r}{l}\right)^2 + (1+2k(1+\nu_s))\left(\frac{t^{(2)}}{l}\right)^2\right] \\ +\left[\frac{3\pi}{2} - 9\sqrt{3}\left(\frac{r}{l}\right) + \left(4\pi + \frac{3\sqrt{3}}{2}\right)\left(\frac{r}{l}\right)^2 + \left(\left(\frac{\pi}{3} + \frac{\sqrt{3}}{8}\right)\right.\right. \\ \left.\left. +2k(1+\nu_s)\left(\frac{\pi}{3} - \frac{\sqrt{3}}{8}\right)\right)\left(\frac{t^{(2)}}{l}\right)^2\right] \end{array}\right\} \\ &\quad + \left(\frac{1}{2} - \frac{r}{l}\right)\left[3\left(\frac{1}{2} - \frac{r}{l}\right)^2 + \frac{1}{4}(1+6k(1+\nu_s))\left(\frac{t^{(2)}}{l}\right)^2\right] + \left(\frac{t^{(2)}}{l}\right)^2 \end{aligned}$$

and thus, the strain ε in the representative unit is calculated:

$$\varepsilon_V = \frac{\Delta_V}{3l/4} = \frac{\sigma}{E^s}\frac{2\sqrt{3}}{3}\left(\frac{l}{t^{(2)}}\right)^3 f\left(\frac{r}{l}, \frac{t^{(2)}}{l}\right) \quad (9)$$

Finally, the Young's modulus is obtained:

$$\frac{E^{(2)}}{E^s} = \frac{\sqrt{3}}{2}\left(\frac{t^{(2)}}{l}\right)^3 f^{-1}\left(\frac{r}{l}, \frac{t^{(2)}}{l}\right) \quad (10)$$

if r/l tends to zero, and the quadratic term $(t^{(2)}/l)^2$ in $f(r/l, t^{(2)}/l)$ is neglected due to its smallness (*i.e.*, the shear and axial deformations are neglected), then, $f(r/l, t^{(2)}/l)$ approach 3/8, and more, Eq. (10) will be rewritten as $E^{(2)}/E^s = 2.3(t^{(2)}/l)^3$, which is the result of the conventional regular hexagonal honeycomb reported in Ref. [17].

2.2. Poisson's ratio

In Eq. (3), if we exclude M_0 (*i.e.*, let M_0 disappear), $\frac{P_0 l}{M} = \frac{2}{\sqrt{3}}\left(\frac{r}{l}\right)^{-1}$ holds, and the strain energy is now defined as $\overline{U}_{AD}$, which is expressed as:

$$\overline{U}_{AD}=\frac{P_0^2 r}{2E^s A^{(2)}}\left(\frac{t^{(2)}}{l}\right)^{-2} \times \left[\begin{array}{l} 12\left(\frac{r}{l}\right)^2\left(\frac{3\pi}{4}\lambda_2^2+\left(\pi-\frac{3\sqrt{3}}{2}\right)\lambda_2-\frac{3\pi}{2}\left(\frac{r}{l}\right)\lambda_1\lambda_2\right) \\ +\frac{\sqrt{3}}{2}\left(\frac{r}{l}\right)\lambda_1\left((27-8\sqrt{3})\left(\frac{r}{l}\right)^2+\frac{3}{4}(1-2k(1+v_s))\left(\frac{t^{(2)}}{l}\right)^2\right) \\ +\frac{3\pi}{8}\left(\frac{r}{l}\right)^2\lambda_1^2\left(36\left(\frac{r}{l}\right)^2+(1+2k(1+v_s))\left(\frac{t^{(2)}}{l}\right)^2\right) \\ +\left(10\pi-\frac{33\sqrt{3}}{2}\right)\left(\frac{r}{l}\right)^2+\left(\left(\frac{\pi}{3}+\frac{\sqrt{3}}{8}\right)+2k(1+v_s)\left(\frac{\pi}{3}-\frac{\sqrt{3}}{8}\right)\right)\left(\frac{t^{(2)}}{l}\right)^2 \end{array}\right] \tag{11}$$

then, $\overline{U}_{AD}, U_{AD}$, and M_0 should satisfy:

$$\varphi=\frac{U_{AD}-\overline{U}_{AD}}{M_0} \tag{12}$$

where φ is the angular displacement caused by M_0, see Fig. 2. According to the structural analysis in Fig. 2, the displacements caused by the shear and axial forces in part BC are:

$$\delta_V=\frac{2}{\sqrt{3}}\frac{P_0 r}{E^s A^{(2)}}\left(\frac{t^{(2)}}{l}\right)^{-2}\left(\frac{l}{2r}-1\right)\left[3\left(\frac{1}{2}-\frac{r}{l}\right)^2+\frac{3}{2}k(1+v_s)\left(\frac{t^{(2)}}{l}\right)^2\right]$$
$$\delta_N=\frac{1}{2}\frac{P_0 r}{E^s A^{(2)}}\left(\frac{l}{2r}-1\right) \tag{13}$$

Therefore, the horizontal displacement of the point C is calculated as:

$$\Delta_H=-\varphi\left(\frac{l}{2}-r\right)\sin\frac{\pi}{6}-\delta_V\sin\frac{\pi}{6}+\delta_N\cos\frac{\pi}{6} \tag{14}$$

Finally, the Poisson's ratio is obtained as:

$$v=-\frac{\varepsilon_H}{\varepsilon_V}=-\frac{\Delta_H/(\sqrt{3}l/4)}{\Delta_V/(3l/4)}=-\frac{\sqrt{3}\Delta_H}{\Delta_V} \tag{15}$$

2.3. Fracture strength and stress intensity factor

In this section, we consider two fracture mechanisms in an imperfect honeycomb (Fig. 3) as stated in the literature [15]. One is that the crack propagates due to the tensile-bending failure of the vertical cell wall (Fig. 3b), and the other is due to the bending failures of the curved cell wall ($B'D'$ in Fig. 3c) of the circular joint and the inclined cell walls ($B'C'$ in Fig. 3d). For the two mechanisms, their fracture strengths and stress intensity factors are derived, respectively, and the competition between them, like that in Ref. [18], is discussed.

2.3.1. Mechanism (1): tensile-bending failure of the vertical cell wall

According to Choi and Sankar [15], the axial force P_E and moment M_E acting on the first cell wall ahead of crack tip are expressed as,

$$P_E=\int_0^a\frac{K_I}{\sqrt{2\pi r}}b dr=K_I b\sqrt{\frac{2a}{\pi}}$$
$$M_E=\int_0^a\frac{K_I}{\sqrt{2\pi r}}b r dr=\frac{K_I b}{3}\sqrt{\frac{2a^3}{\pi}} \tag{16}$$

where $a=\zeta l$ is an effective length, $\zeta=0.411(\bar{\rho}^{(2)})^{0.308}$ [15] is a dimensionless factor, K_I is the mode-I stress intensity factor. If the failure of the vertical cell wall occurs, the maximum bending stress $\sigma_{\max}$ in the cell wall produced by the forces should equal the tensile strength σ_{cr}^s of the cell wall materials, *i.e.*,

$$\sigma_{cr}^s=\frac{P_E}{bt^{(2)}}+\frac{6M_E}{b(t^{(2)})^2}=K_{IC,1}^{(2)}\left(\frac{l}{t^{(2)}}\right)^2\sqrt{\frac{2\zeta}{\pi l}}\left(\frac{t^{(2)}}{l}+2\zeta\right) \tag{17}$$

where $K_{IC,1}^{(2)}$ is the critical stress intensity factor, in which the second subscript 1 denotes the first failure mechanism. Then, rearranging Eq. (17), the stress intensity factor is obtained as,

$$\frac{K_{IC,1}^{(2)}}{\sigma_{cr}^s\sqrt{\pi l}}=\frac{1}{\sqrt{2\zeta}\left(\frac{t^{(2)}}{l}+2\zeta\right)}\left(\frac{t^{(2)}}{l}\right)^2 \tag{18}$$

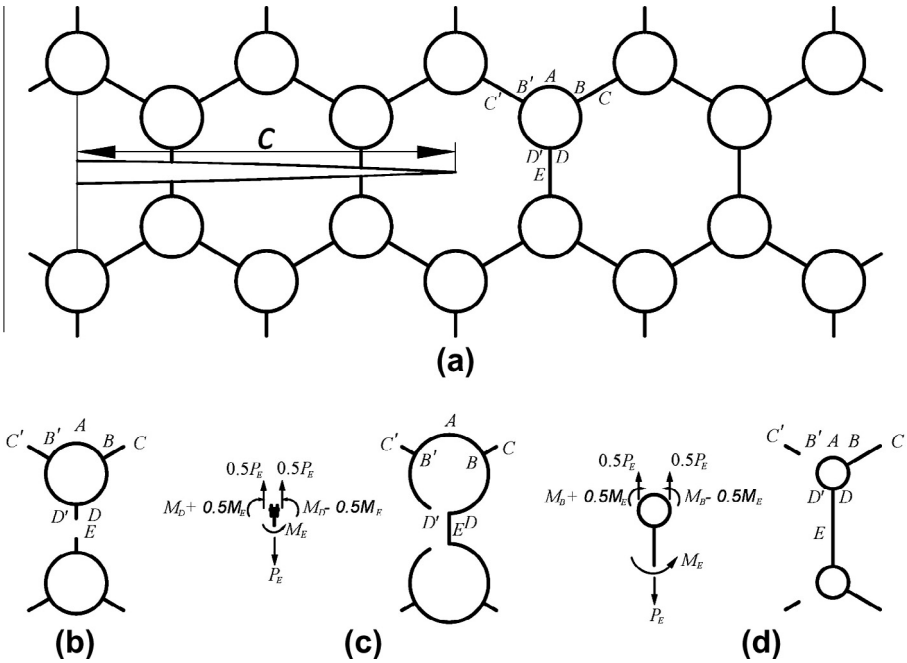

Fig. 3. (a) Preexisting crack in the honeycomb; (b) fracture in vertical cell walls; (c) fracture at the point D' and force analysis; (d) fracture at the point B' and force analysis.

The quantized fracture mechanics (QFM) presented by Pugno [19,20], has already been applied to carbon nanotubes and graphene. Thanks to the geometric similarity between the present structure and graphene, QFM is employed here to derive the honeycomb's fracture strength. If a preexisting crack with length $2c$ exists in the honeycomb (Fig. 3a), the effective length a is defined as the fracture quanta, then, the QFM strength of the honeycomb is expressed as $\sigma_{cr,1}^{(2)} = K_{IC,1}^{(2)}/\sqrt{\pi(c+a/2)}$. Furthermore, we assume that the crack length satisfies $2c = n\sqrt{3}l$, where n is the number of cracked cells, then, the strength of the honeycomb is expressed,

$$\frac{\sigma_{cr,1}^{(2)}}{\sigma_{cr}^{s}} = \frac{1}{\sqrt{\zeta}\left(\frac{t^{(2)}}{l}+2\zeta\right)\sqrt{\sqrt{3}n+\zeta}}\left(\frac{t^{(2)}}{l}\right)^2 \tag{19}$$

2.3.2. Mechanism (2): bending failure of cell walls

Before discussing the bending failure mechanism, let us study the strength of a perfect honeycomb first. Its strength is reached when a cell wall fails due to the maximum bending moment. We can see that the moment at the end B (or B' due to symmetry) of the beam BC (or $B'C'$) gradually disappears if the ratio r/l approaches 0.5, and the position of the maximum moment switches from the end B (or B') of the oblique cantilever beam BC (or $B'C'$) to the end D (or D') of the semicircle AD. According to the force analysis with above-obtained reaction forces R and M_A, and denoting the maximum moments at the two positions as M_B (or $M_{B'}$) and M_D (or $M_{D'}$), respectively, the dimensionless moments are expressed as:

$$\begin{cases} \frac{M_B}{P_0 l} = \frac{\sqrt{3}}{2}\left(\frac{1}{2}-\frac{r}{l}\right) \\ \frac{M_D}{P_0 l} = \frac{\sqrt{3}}{4}\left[\lambda_2 - 2\lambda_1\left(\frac{r}{l}\right)+1\right] \end{cases} \tag{20}$$

Second, for an imperfect honeycomb, the fracture location locates at the points B' or D'. For these two cases, the force analysis are shown in Fig. 3c and d, respectively. It is noted that 0.5 P_E in Fig. 3c and d corresponds to P_0 in Fig. 2, and thus, substituted P_0 in Eq. (20) with $0.5P_E$, the bending moment at the points B' or D' in the cracked honeycomb can be expressed as,

$$\begin{cases} \frac{M_{B'}}{P_E l} = \frac{M_B + 0.5M_E}{P_E l} = \frac{\sqrt{3}}{4}\left(\frac{1}{2}-\frac{r}{l}\right)+\frac{\zeta}{6} \\ \frac{M_{D'}}{P_E l} = \frac{M_D + 0.5M_E}{P_E l} = \frac{\sqrt{3}}{8}\left[\lambda_2 - 2\lambda_1\left(\frac{r}{l}\right)+1\right]+\frac{\zeta}{6} \end{cases} \tag{21}$$

where M_B and M_D, which can be calculated by Eq. (20), are bending moments at the points B' or D' caused only by the axial force P_E thanks to the structural symmetry. For brittle materials, the maximum moment $M_{\max} = \frac{1}{6}\sigma_{cr}^{s} b (t^{(2)})^2$, thus, the failure occurs when $M_{\max} = \max(M_{B'}, M_{D'})$, then, we find,

$$\frac{K_{IC,2}^{(2)}}{\sigma_{cr}^{s}\sqrt{\pi l}} = \begin{cases} \frac{1}{\sqrt{2\zeta}\left[\frac{3\sqrt{3}}{2}\left(\frac{1}{2}-\frac{r}{l}\right)+\zeta\right]}\left(\frac{t^{(2)}}{l}\right)^2 & M_{D'} < M_{B'} \\ \frac{1}{\sqrt{2\zeta}\left[\frac{3\sqrt{3}}{4}\left(\lambda_2 - 2\lambda_1\left(\frac{r}{l}\right)+1\right)+\zeta\right]}\left(\frac{t^{(2)}}{l}\right)^2 & M_{D'} > M_{B'} \end{cases} \tag{22}$$

similarly, the strength is derived by QFM,

$$\frac{\sigma_{cr,2}^{(2)}}{\sigma_{cr}^{s}} = \begin{cases} \frac{1}{\sqrt{\zeta}\left[\frac{3\sqrt{3}}{2}\left(\frac{1}{2}-\frac{r}{l}\right)+\zeta\right]\sqrt{\sqrt{3}n+\zeta}}\left(\frac{t^{(2)}}{l}\right)^2 & M_{D'} < M_{B'} \\ \frac{1}{\sqrt{\zeta}\left[\frac{3\sqrt{3}}{4}\left(\lambda_2 - 2\lambda_1\left(\frac{r}{l}\right)+1\right)+\zeta\right]\sqrt{\sqrt{3}n+\zeta}}\left(\frac{t^{(2)}}{l}\right)^2 & M_{D'} > M_{B'} \end{cases} \tag{23}$$

considering the limiting case that r/l tends to zero and $\zeta = 1$, then, $M_D < M_B$ holds and Eq. (22) becomes $K_{IC,2}^{(2)} = 0.307\sigma_{cr}^{s}\sqrt{\pi l}\left(\frac{t^{(2)}}{l}\right)^2$, which is identical to the result of the stress intensity factor of regular hexagonal honeycombs in Ref. [17]; and more, if $n = 0$, Eq. (23) becomes $\frac{\sigma_{cr,2}^{(2)}}{\sigma_{cr}^{s}} = 0.435\left(\frac{t^{(2)}}{l}\right)^2 \approx \frac{4}{9}\left(\frac{t^{(2)}}{l}\right)^2$, which is also the result of the compressive strength of perfect regular hexagonal honeycombs in Ref. [17].

Overall, as the ratio r/l varies, the fracture location changes. For the whole structure, its strength $\sigma_{cr}^{(2)}$ can be determined by $\sigma_{cr}^{(2)} = \min(\sigma_{cr,1}^{(2)}, \sigma_{cr,2}^{(2)})$ according to Eqs. (19) and (23). Correspondingly, its stress intensity factor $K_{IC}^{(2)}$ is also obtained by minimizing Eqs. (18) and (22), *i.e.*, $K_{IC}^{(2)} = \min(K_{IC,1}^{(2)}, K_{IC,2}^{(2)})$.

3. Results and discussion

Here, we study the influences of the relative density and parameter r/l on the Young's modulus, Poisson's ratio, fracture strength and stress intensity factor of the honeycomb normalized by its counterparts of the conventional regular hexagonal honeycomb. The Poisson's ratio v_s of the constituent material is assumed to be 0.3. The range for r/l is from 0.1 to 0.45 and $\bar{\rho}^{(2)}$ is set in the range from 0.01 to 0.21, then, according to Eq. (1) and r/l, we find $t^{(2)}/r$ varying from 0.001 to 1.741, which satisfies the conditions $0 < t^{(2)}/r < 2$.

For the normalized Young's modulus, we compare the result of the present structure by the theory with those of the similar structure studied by experiments and finite element results [11], and parametrically investigate the influences of the relative density and r/l. The structure in Ref. [11] is controlled by the ratio a/l, in which a is the side length of the hexagon (see Fig. 4a). The results are reported in Fig. 4. We can see that the present theory (the line in Fig. 4a) agrees well with the experimental (the circle in Fig. 4a) and finite element results (the square in Fig. 4a) even though they have different geometries. The former has an optimal value when $r/l \approx 0.31$, which is less than the latter's optimal value when $a/l \approx 0.33$, this is because r is less than a if a hexagon is equivalent to a circle. The parametric study shows that the optimal value, with respect to the conventional honeycomb, decreases (Fig. 4b) as the relative density increases, and the normalized Young's modulus tends to one, as r/l approaches 0.1 which means that the Young's modulus of the honeycomb tends to that of the conventional honeycomb. Corresponding to the conventional honeycomb, the improvement of the Young's modulus is up to 76% when $\bar{\rho}^{(2)} = 0.01$ and $r/l = 0.31$.

For the structure's Poisson's ratio, the present prediction is also compared with the finite element results reported in Ref. [11], and a good agreement is again obtained, see Fig. 5a. If $r/l \to 0.1$, the Poisson's ratio tend to the well-known result (*i.e.*, one), and a lowest value $v = 0.315$ is reached when $r/l = 0.38$, which is less than the reported value 0.37 when $a/l = 0.4$ under the common relative density $\bar{\rho}^{(2)} = 0.06$. The reason can be referred to the corresponding discussion of Young's modulus. The parametric study on the Poisson's ratio is performed with respect to the relative density and r/l, and the result is plotted in Fig. 5b, which shows that the Poisson's ratio is between 0.313 and 0.996.

For the fracture strength, the mechanism (1) is absent and the mechanism (2) prevails, thus, the fracture location switches from the point B' to the point D' (Fig. 6a). Interestingly, if the bending failure occurs at the point B', it reaches a minimum when $r/l \approx 0.25$. This is because a smaller r results in a greater cell-wall thickness $t^{(2)}$, which requires a greater bending moment to fail; a greater r results in a smaller moment arm of the beam $B'C'$, which also needs a greater force to fail, and $r \approx 0.25l$ is in-between. Whereas, if the failure is at the point D', an increasing r results in a decreasing $t^{(2)}$, thus, the failure bending moment becomes smaller and smaller. Moreover, as the number of cracked cells (or crack length) increases, the normalized fracture strength increases (Fig. 6b). This is because the fracture quanta plays a more important role in the case of a shorter crack which reduces the

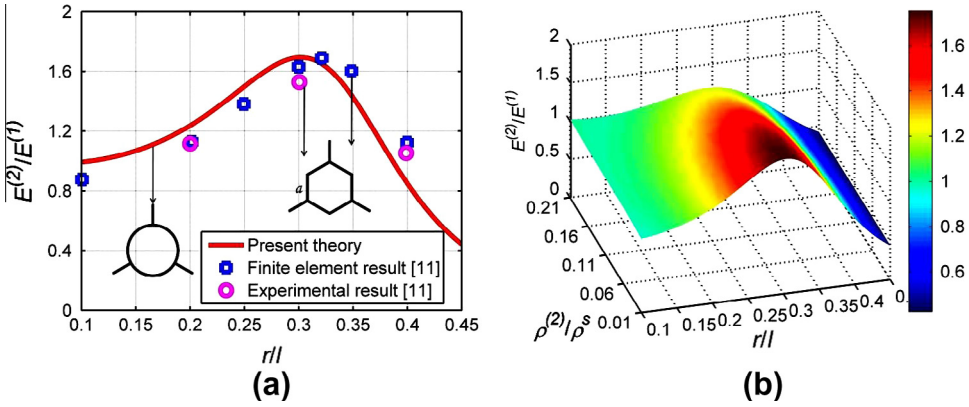

Fig. 4. (a) Comparison between the present theory of the present structure, experiments and finite element results from the literature [11], when $\bar{\rho}^{(2)} = \bar{\rho}^{(1)} = 0.1$; (b) normalized Young's modulus *vs.* relative density $\bar{\rho}^{(2)}$ and r/l.

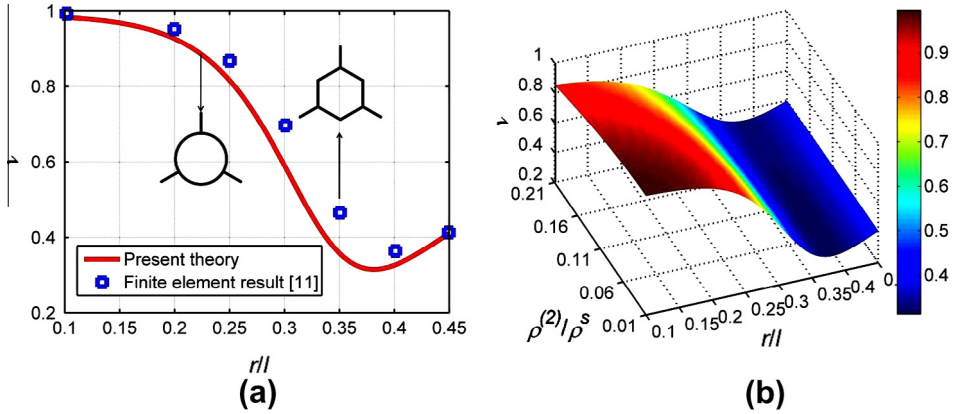

Fig. 5. (a) Comparison between the present theory of the present structure and finite element results from the literature [11], when $\bar{\rho}^{(2)} = \bar{\rho}^{(1)} = 0.06$; (b) Poisson's ratio *vs.* relative density $\bar{\rho}^{(2)}$ and r/l.

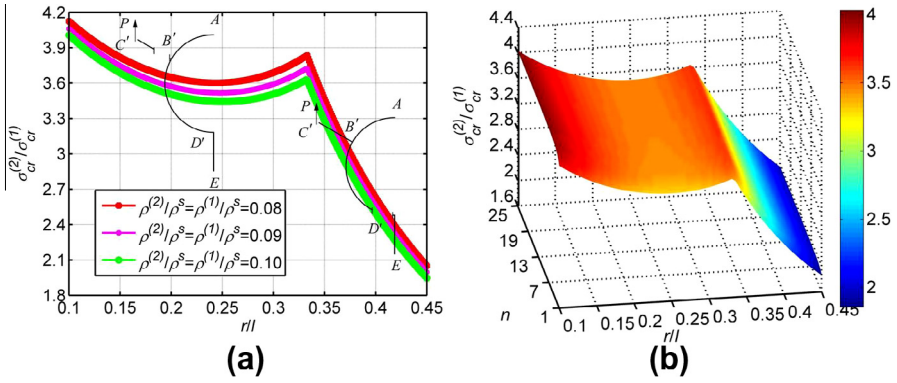

Fig. 6. (a) Normalized fracture strength *vs.* r/l when $n = 7$; (b) normalized fracture strength *vs.* number of cracked unit cells n and r/l when $\bar{\rho}^{(2)} = \bar{\rho}^{(1)} = 0.1$.

improvement of the fracture strength, and its influence weakens as the crack length increases. In particular, the maximal improvement of the fracture strength with respect to the conventional honeycomb is up to 300% when $r/l = 0.1$ and $n = 25$, and for each n, the maximal improvement is always reached at $r/l = 0.1$. It is worth mentioning that the critical failure at both points B' and D' occurs simultaneously when $r/l = 0.33$, and its strength is improved by 264% when $r/l = 0.33$ and $n = 25$.

Finally, the result of the stress intensity factor is reported in Fig. 7. Different from the optimal value of the Young's modulus when $r/l = 0.31$ (Fig. 4b) and the maximal value of the fracture strength when $r/l = 0.1$ (Fig. 6b), the maximal value of the normalized stress intensity factor varies from $r/l = 0.1$ to $r/l = 0.33$ as the relative density decreases. Addressing this point, we study its critical conditions depicted in Fig. 7a. It shows that the maximal value appears at both $r/l = 0.1$ and $r/l = 0.33$ when $\bar{\rho}^{(2)} = 0.03$; while it is at $r/l = 0.33$ when $\bar{\rho}^{(2)} = 0.02$ and at $r/l = 0.1$ when $\bar{\rho}^{(2)} = 0.04$. Therefore, combining Fig. 7b, it can be concluded that the maximal value of the normalized stress intensity factor is at $r/l = 0.33$ if $\bar{\rho}^{(2)} < 0.03$ while at $r/l = 0.1$ if $\bar{\rho}^{(2)} > 0.03$. Compared to the

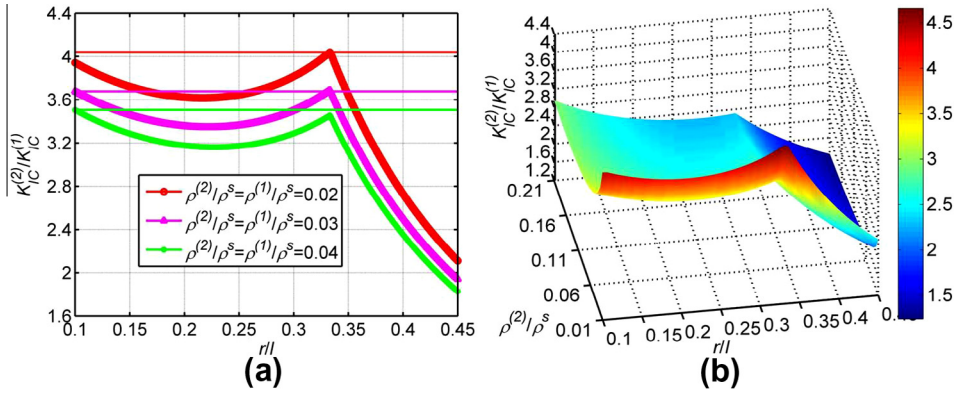

Fig. 7. (a) Normalized stress intensity factor *vs.* r/l, note that the three horizontal lines are corresponding to the maximal values of the three cases, respectively; (b) normalized fracture strength *vs.* relative density $\bar{\rho}^{(2)}$ and r/l.

conventional regular honeycomb, the stress intensity factor is maximally improved by 366% when $\bar{\rho}^{(2)} = 0.01$ and $r/l = 0.33$ and by 195% when $\bar{\rho}^{(2)} = 0.21$ and $r/l = 0.1$. It is worth mentioning that if the natural honeycomb has a relative density greater than 0.03, the result illustrates why more silk and wax are centrally located at the three-edge joint, according to strength and fracture toughness of which the maximal values are at smaller r/l.

4. Conclusion

In this paper, we have constructed a hollow-cylindrical-joint honeycomb, and developed a theory to calculate its Young's modulus, Poisson's ratio, fracture strength and stress intensity factor. With respect to the conventional honeycomb, the results showed that its Young's modulus can be optimized and comparable to that in the literature. The smallest Poisson's ratio is obtained when $r/l \approx 0.38$. For the maximal improvement of its fracture strength, it can be obtained by decreasing the radius of the circular joint. Whereas, a critical relative density 0.03 exists for the maximal improvement of stress intensity factor, namely, the maximal value is reached when the ratio r/l equals 0.1 and the honeycomb's relative density is greater than 0.03; otherwise, the maximal value is obtained when r/l equals 0.33 and the honeycomb's relative density is less than 0.03. The present structure and theory could be used as a guide to design new honeycomb materials.

Acknowledgements

CQ is supported by the Priority Academic Program Development of Jiangsu Higher Education Institutions (No. 1107037001) and the National Natural Science Foundation of China (NSFC) (No. 31300780). NP thanks the European Research Council (ERC StG Ideas 2011 BIHSNAM, ERC Proof of Concept REPLICA2 2013) and the European Union (Graphene Flagship) for support.

References

[1] Zhang K, Duan HL, Karihaloo BL, Wang JX. Hierarchical, multilayered cell walls reinforced by recycled silk cocoons enhance the structural integrity of honeybee combs. Proc Natl Acad Sci USA 2010;107:9502–6.
[2] Chen Q, Pugno NM. Bio-mimetic mechanisms of natural hierarchical materials: a review. J Mech Behav Biomed Mater 2013;19:3–33.
[3] Evans AG, Hutchinson JW, Fleck NA, Ashby MF, Wadley HND. The topological design of multifunctional cellular metals. Prog Mater Sci 2001;46:309–27.
[4] Zheng Q, Fan H, Liu J, Ma Y, Yang L. Hierarchical lattice composites for electromagnetic and mechanical energy absorptions. Compos Part B – Eng 2013;53:152–8.
[5] Zheng J, Zhao L, Fan H. Energy absorption mechanisms of hierarchical woven lattice composites. Compos Part B – Eng 2012;43:1516–22.
[6] Sun Y, Chen Q, Pugno N. Elastic and transport properties of the tailorable multifunctional hierarchical honeycombs. Compos Struct 2014;107:698–710.
[7] Chen Q, Pugno NM. Mechanics of hierarchical 3-D nanofoams. EPL 2012;97:26002.
[8] Chen Q, Pugno NM. In-plane elastic buckling of hierarchical honeycomb materials. Eur J Mech A/Solids 2012;34:120–9.
[9] Fan H, Jin F, Fang D. Mechanical properties of hierarchical cellular materials. Part I Analysis. Compos Sci Technol 2008;68:3380–7.
[10] Taylor CM, Smith CW, Miller W, Evans KE. The effects of hierarchy on the in-plane elastic properties of honeycombs. Int J Solids Struct 2011;48:1330–9.
[11] Ajdari A, Jahromi BH, Papadopoulos J, Nayeb-Hashemi H, Vaziri A. Hierarchical honeycombs with tailorable properties. Int J Solids Struct 2012;49:1413–9.
[12] Sun Y, Pugno N. In plane stiffness of multifunctional hierarchical honeycombs with negative Poisson's ratio substructures. Compos Struct 2013;106:681–9.
[13] Maiti SK, Ashby MF, Gibson LJ. Fracture toughness of brittle cellular solids. Scripta Metall 1984;18:213–7.
[14] Choi JB, Lakes RS. Fracture toughness of re-entrant foam materials with a negative Poisson's ratio: experiment and analysis. Int J Fract 1996;80:73–83.
[15] Choi S, Sankar BV. A micromechanical method to predict the fracture toughness of cellular materials. Int J Solids Struct 2005;42:1797–817.
[16] Miller W, Smith CW, Scarpa F, Evans KE. Flatwise buckling optimization of hexachiral and tetrachiral honeycombs. Compos Sci Technol 2010;70:1049–56.
[17] Gibson LJ, Ashby MF. Cellular solids: structure and properties. 2nd ed. Cambridge: Cambridge University Press; 1997.
[18] Chen Q, Pugno NM. Competition between in-plane buckling and bending collapses in nanohoneycombs. Europhys Lett 2012;98:16005.
[19] Pugno NM, Ruoff RS. Quantized fracture mechanics. Philos Mag 2004;84:2829–45.
[20] Pugno NM. Dynamic quantized fracture mechanics. Int J Fract 2006;140:159–68.